Spectrochimica Acta Part A: Molecular and Biomolecular Spectroscopy 136 (2015) 1216–1226

Contents lists available at ScienceDirect

Spectrochimica Acta Part A: Molecular and Biomolecular Spectroscopy

journal homepage: www.elsevier.com/locate/saa

Structural, spectroscopic and theoretical studies of dimethylphenyl betaine complex with two molecules of 2,6-dichloro-4-nitro-phenol

Mirosław Szafran *, Anna Komasa, Kinga Ostrowska, Andrzej Katrusiak, Zofia Dega-Szafran

Faculty of Chemistry, Adam Mickiewicz University, Grunwaldzka 6, 60780 Poznań, Poland

HIGHLIGHTS

- Dimethylphenyl betaine crystallizes with two molecules of 2,6-dichloro-4-nitro-phenol.
- Molecules are linked by two different O—H···O hydrogen bonds without the proton transfer.
- The structures in crystal, gas phase and DMSO solution are analyzed.
- The experimental and calculated frequencies have been assigned.
- The magnetic isotropic shielding constants reproduce the experimental chemical shifts.

GRAPHICAL ABSTRACT

The 1:2 complex of dimethylphenyl betaine with two molecules of 2,6-dichloro-4-nitro-phenol was prepared and investigated by X-ray diffraction, B3LYP/6-311++G(d,p) and B3LYP-D3/6-311++G(d,p) calculations, FTIR and NMR spectroscopies. Phenols are bonded to each oxygen atoms of COO^- group of the betaine by two nonequivalent O···H—O hydrogen bonds of 2.473(5) and 2.688(4) Å.

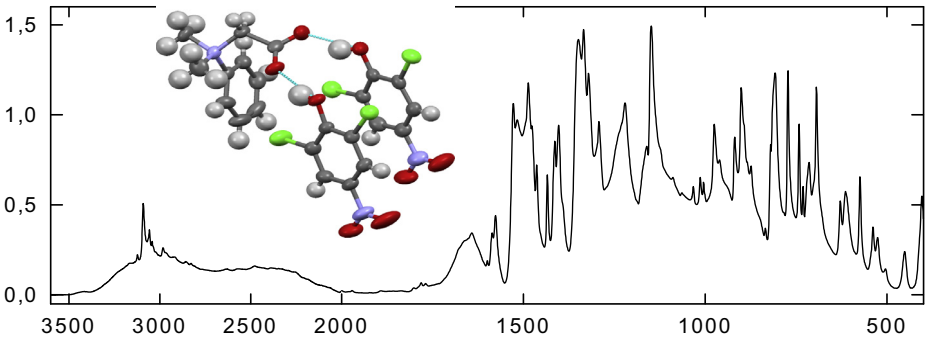

ARTICLE INFO

Article history:
Received 29 April 2014
Received in revised form 21 July 2014
Accepted 8 October 2014
Available online 16 October 2014

Keywords:
Dimethylphenyl betaine
2,6-Dichloro-4-nitro-phenol
X-ray diffraction
FTIR and NMR spectra
B3LYP calculations
Hydrogen bonds

ABSTRACT

The 1:2 complex (**1**) of dimethylphenyl betaine (DMPB) with two molecules of 2,6-dichloro-4-nitro-phenol (DCNP) was prepared and characterized by X-ray diffraction, B3LYP/6-311++G(d,p) and B3LYP-D3/6-311++G(d,p)calculations, FTIR and NMR spectroscopies. The crystal is monoclinic, space group $P2_1/c$ with $Z = 4$. The protons at the oxygen atoms of phenols are bonded to each oxygen atoms of the DMPB carboxylate group by two nonequivalent H-bonds with the O—H···O distances of 2.473(5) and 2.688(4) Å. Both H-bonds in the optimized structures **2** (in vacuum), **3** (in DMSO solution) and dispersion-correlated functional (D3) **4** (in vacuum) are comparable and are slightly shorter than O(6)—H(O6)···O(2) in the crystal. The FTIR spectrum of **1** shows a broad absorption in the 3400–2000 cm^{-1} region corresponding to a longer hydrogen bond and a broad absorption in the 1800–500 cm^{-1} region caused by the shorter H-bond. The relations between the experimental ^{13}C and ^{1}H chemical shifts (δ_{exp}) of the investigated compound **1** in DMSO solution and GIAO/B3LYP/6-311++G(d,p) magnetic isotropic shielding constants (σ_{calc}) obtained by using the screening solvation model (COSMO) for **3** are linear and reproduce well the experimental chemical shifts described by the equation: $\delta_{exp} = a + b\ \sigma_{calc}$.

* Corresponding author. Tel.: +48 61 8291320; fax: +48 51 8291555.
E-mail address: szafran@amu.edu.pl (M. Szafran).

http://dx.doi.org/10.1016/j.saa.2014.10.007
1386-1425/

Introduction

Among many various kinds of molecular interactions, the hydrogen bond has a special position. The hydrogen bond is of great importance in natural sciences, chemistry, physics and biochemical processes. Hence, its nature is often the subject of investigation and polemics [1–9]. Interesting hydrogen bonds are in complexes of betaines with mineral and organic acids [10].

Betaines are compounds with oppositely charged centers and are often referred to as zwitterions, inner salts, dipolar ions or salt-bridged-containing molecules. This diverse nomenclature reflects the extraordinary importance of these species in biological transformations, organic synthesis, preparation of novel materials and as chromatographic supports [10–12]. Betaine [$(CH_3)_3N^+CH_2COO^-$] is distributed in animals, plants, microorganisms and is a significant component of many food products [13]. In betaines [$(R_3N^+CH_2COO^-$] the quaternary nitrogen atom is inert as a hydrogen bond center, whereas the carboxylate group is basic and can interact with different proton donors. The nitrogen atom can be surrounded by alkyl groups or be involved in heteroaliphatic or heteroaromatic rings [10].

Betaines form 1:1 and 2:1 complexes with mineral and organic acids [14,15] and phenols [16]. Recently, we have described a third type of complex (1:2) of pyridine betaine with two molecules of 2,6-dichloro-4-nitro-phenol (DCNP) [17] and pentachlorophenol [18]. In this study, we have synthesized another 1:2 complex of dimethylphenyl betaine with two molecules of 2,6-dichloro-4-nitro-phenol.

Experimental and calculations

Dimethylphenyl betaine (DMPB) was prepared according to the method described in Ref. [19]. When mixing stoichiometric amount of DMPB with 2,6-dichloro-4-nitro-phenol (DCNP) in methanol only the 1:2 complex, DMPB·$(DCNP)_2$, is formed. Thus the best method of synthesis is mixing the components at the 1:2 ratio. The obtained complex was recrystallized from methanol, m.p. 138 °C. Analysis for $C_{22}H_{19}Cl_4N_3O_8$; calculated: C, 44.39%; H, 3.22%; N, 7.06%; found: C, 44.37%; H, 3.25%; N, 7.08%. The deuterated complex was prepared by a twofold dissolution in D_2O with subsequent removal of the solvent under reduced pressure. The residue was recrystallized from CH_3OD.

FTIR spectra were recorded in Nujol and Fluorolube mulls on Bruker IFS 66v/S spectrometer, evacuated to avoid water and CO_2 absorptions at 2 cm^{-1} resolution. Each FTIR spectrum was accumulated by acquisition of 64 scans. The Raman spectrum of crystalline sample was measured on a Bruker FRA-106/S instrument operating at the 1064 nm exciting line of Nd:YAG laser with the resolution of 1 cm^{-1}. The spectrum was accumulated by acquisition of 200 scans.

NMR spectra were recorded using a Varian VNMRS-400 spectrometer operating at 402.6435 and 101.2440 MHz for ^1H and ^{13}C, respectively. The ^1H and ^{13}C chemical shifts were measured in DMSO-d_6 solution relative to TMS. The chemical shifts were confirmed by COSY and HETCOR experiments.

The X-ray diffraction measurements on the crystal of **1** were carried out on an Oxford Diffraction Excalibur EOS-CCD diffractometer. The structure was solved by direct methods with SHELXS-97 and refined by full-matrix least-squares with SHELXL-97 [20]. The H-atoms were located on the basis of geometry (methyl C—H 0.97 Å, phenyl 0.93 Å, methylene 0.96 Å). The anisotropic thermal parameters were refined for the non-H-atoms, and isotropic U_{iso} parameters for H atoms were linked to U_{eq} of their carriers. The crystal data, together with the details concerning the data collection and structure refinement are given in Table 1 and the atomic coordinates are in Table S1 in Supplementary Material. The crystal data have been deposited in the Cambridge Crystallographic Database Centre as a Supplementary publication CCDC 992834. Molecular illustrations were prepared using ORTEPII [21] and XP [22] packages.

The calculations were performed using the Gaussian 09 program package [23] and the B3LYP and B3LYP-D3 [24–26] approaches in conjunction with 6-311++G(d,p) basis set [27]. B3LYP-D3 [26] denotes a calculation with the usual B3LYP functional plus a D3 dispersion correlation energy term. The dispersion correlation energy term is a function of interatomic distances and contains adjustable parameters that are filled to conformational and interaction energies computed using CCSD(T)/CBS. The vibrational FTIR spectra (harmonic wavenumbers and absolute intensities) were calculated at the B3LYP/6-311++G(d,p) level of theory. The calculated IR frequencies were positive and confirmed that the optimized structures were in the states of minimum energies. The magnetic isotropic shielding constants were calculated using the standard GIAO/B3LYP/6-311++G(d,p) (Gauge-Independent Atomic Orbital) approach with the Gaussian 09 program package using the conductor-like screening solvation model (COSMO) [28–32].

Results and discussion

Crystal structure

The crystals of the 1:2 complex of dimethylphenyl betaine (DMPB) with 2,6-dichloro-4-nitro-phenol (DCNP) (**1**) belong to monoclinic system, space group $P2_1/c$. The selected bond lengths, bond and torsion angles are listed in Table 2. The molecular structure and labeling scheme are shown in Fig. 1, while the crystal packing is presented in Fig. 2. In the investigated complex both phenol molecules (DCNP) form two nonequivalent hydrogen bonds with the DMPB carboxylate group with the O—H···O distances of 2.473(5) and 2.688(4) Å without proton transfer (Table 3). The O···O distances are comparable with those found in the 1:2 complex of pyridine betaine with DCNP [17], however in this complex pyridine betaine is protonated and the O···H—O distances are

Table 1
Crystal data and structure refinement of the 1:2 complex of dimethylphenyl betaine with 2,6-dichloro-4-nitro-phenol.

Empirical formula	$C_{22}H_{19}Cl_4N_3O_8$
Formula weight	595.20
Temperature	296(2) K
Wavelength	0.71073 Å
Crystal system	Monoclinic
Space group	$P2_1/c$
Unit cell dimensions	a = 16.6511(5) Å
	b = 11.6487(5) Å
	c = 13.3614(6) Å
	β = 105.864(4)°
Volume	2492.92(17) $Å^3$
Z	4
Calculated density	1.586 g cm^{-3}
Absorption coefficient	0.529 mm^{-1}
$F(000)$	1216
Crystal size	0.30 × 0.30 × 0.10 mm
θ range for data collection	3.48–27.58°
Max/min. indices h, k, l	$-12 \leqslant h \leqslant 21$, $-14 \leqslant k \leqslant 15$, $-16 \leqslant l \leqslant 16$
Reflections collected/unique	10,547/5267 R_{int} = 0.0334
Completeness to θ_{max} = 29.9%	91.3%
Refinement method	Full-matrix least-squares on F^2
Data/restraints/parameters	5267/0/341
Goodness-of-fit on F^2	1.004
Final R indices [$I > 2\sigma_I$]	R_1 = 0.0641, wR_2 = 0.1243
R indices (all data)	R_1 = 0.0960, wR_2 = 0.1555
Largest diff. peak and hole	0.362 and −0.351 e.A^{-3}

Table 2
Selected experimental and calculated bond lengths (Å), bond and torsion angles (°) for the 1:2 complex of dimethylphenyl betaine with 2,6-dichloro-4-nitro-phenol.

Parameters	X-ray	B3LYP/6-311++G(d,p)		B3LYP-D3/6-311++G(d,p)
	1	**2** (vacuum)	**3** (DMSO)	**4** (vacuum)
Bond lengths				
N(1)—C(1)	1.504(5)	1.5095	1.5086	1.5041
N(1)—C(7)	1.525(5)	1.5110	1.5188	1.5061
N(1)—C(8)	1.502(5)	1.5111	1.5119	1.5084
N(1)—C(9)	1.515(5)	1.5367	1.5271	1.5315
C(1)—C(2)	1.364(5)	1.3893	1.3903	1.3878
C(2)—C(3)	1.383(6)	1.3941	1.3952	1.3952
C(3)—C(4)	1.363(7)	1.3906	1.3915	1.3910
C(4)—C(5)	1.358(7)	1.3923	1.3933	1.3953
C(5)—C(6)	1.385(6)	1.3918	1.3925	1.3914
C(1)—C(6)	1.385(5)	1.3935	1.3938	1.3931
C(9)—C(10)	1.539(5)	1.5548	1.5416	1.5530
C(10)—O(1)	1.257(5)	1.2424	1.2549	1.2419
C(10)—O(2)	1.230(5)	1.2479	1.2549	1.2501
C(11)—C(12)	1.400(6)	1.4134	1.4153	1.4148
C(11)—C(16)	1.395(6)	1.4171	1.4180	1.4173
C(11)—O(3)	1.321(5)	1.3206	1.3187	1.3207
C(12)—C(13)	1.393(6)	1.3840	1.3827	1.3830
C(13)—C(14)	1.365(6)	1.3897	1.3916	1.3897
C(14)—C(15)	1.378(6)	1.3895	1.3939	1.3927
C(15)—C(16)	1.397(6)	1.3812	1.3793	1.3824
C(14)—N(2)	1.454(6)	1.4657	1.4558	1.4627
N(2)—O(4)	1.206(5)	1.2279	1.2309	1.2287
N(2)—O(5)	1.220(5)	1.2268	1.2308	1.2272
C(12)—Cl(1)	1.719(4)	1.7521	1.7500	1.7547
C(16)—Cl(2)	1.719(4)	1.7473	1.7505	1.7438
C(21)—C(22)	1.398(5)	1.4118	1.4140	1.4115
C(21)—C(26)	1.397(5)	1.4145	1.4171	1.4167
C(21)—O(6)	1.341(5)	1.3237	1.3200	1.3235
C(22)—C(23)	1.400(5)	1.3842	1.3827	1.3852
C(23)—C(24)	1.369(6)	1.3897	1.3915	1.3823
C(24)—C(25)	1.377(6)	1.3920	1.3938	1.3915
C(25)—C(26)	1.384(6)	1.3814	1.3795	1.3818
C(24)—N(3)	1.450(5)	1.4671	1.4563	1.4703
N(3)—O(7)	1.217(5)	1.2268	1.2306	1.2260
N(3)—O(8)	1.228(5)	1.2269	1.2306	1.2251
C(22)—Cl(3)	1.721(4)	1.7517	1.7398	1.7556
C(26)—Cl(4)	1.716(4)	1.7485	1.7500	1.7449
Av. dif.[a]		0.0018	−0.017	0.0109
R.m.s.[b]		0.051	0.045	0.015
C(1)—N(1)—C(7)	110.7(3)	108.50	108.13	108.58
C(1)—N(1)—C(8)	112.9(3)	113.05	113.12	113.13
C(1)—N(1)—C(9)	109.4(3)	111.11	111.75	110.19
C(7)—N(1)—C(8)	107.0(3)	107.16	107.09	107.33
C(7)—N(1)—C(9)	106.2(3)	108.31	107.69	108.17
C(8)—N(1)—C(9)	110.5(3)	108.53	108.81	109.20
N(1)—C(1)—C(2)	121.6(4)	121.35	121.03	121.34
N(1)—C(1)—C(6)	117.5(3)	118.10	118.30	117.71
N(1)—C(9)—C(10)	114.4(3)	115.98	117.15	110.19
C(1)—C(2)—C(3)	118.6(4)	119.33	119.31	119.07
C(2)—C(1)—C(6)	120.9(4)	120.53	120.61	120.95
C(1)—C(6)—C(5)	119.1(4)	119.65	119.57	119.48
C(2)—C(3)—C(4)	121.1(4)	120.65	120.63	120.62
C(3)—C(4)—C(5)	120.1(4)	119.54	119.52	119.28
C(4)—C(5)—C(6)	120.1(5)	120.30	120.37	120.20
C(9)—C(10)—O(1)	112.4(4)	111.39	111.93	112.62
C(9)—C(10)—O(2)	119.9(4)	117.45	119.39	116.74
O(1)—C(10)—O(2)	127.7(4)	131.15	128.68	130.64
C(11)—C(12)—C(13)	121.8(4)	122.17	122.08	122.20
C(12)—C(11)—C(16)	117.4(4)	116.42	116.37	116.42
C(11)—C(16)—C(15)	121.0(4)	122.33	122.54	122.14
C(12)—C(13)—C(14)	119.0(4)	118.85	118.90	118.80
C(13)—C(14)—C(15)	121.4(4)	121.56	121.61	121.56
C(14)—C(15)—C(16)	119.4(4)	118.66	118.49	118.75
C(12)—C(11)—O(3)	118.2(4)	125.81	125.65	124.88
C(16)—C(11)—O(3)	124.4(4)	117.71	117.67	118.68
Cl(1)—C(12)—C(11)	118.6(3)	119.22	119.37	119.76
Cl(1)—C(12)—C(13)	119.6(3)	118.61	118.54	118.03
Cl(2)—C(16)—C(11)	120.2(3)	118.41	118.40	118.20
Cl(2)—C(16)—C(15)	118.8(4)	119.25	119.07	118.26
N(2)—C(14)—C(13)	119.2(4)	119.13	119.19	118.89
N(2)—C(14)—C(15)	119.3(4)	119.31	119.20	119.54
C(14)—N(2)—O(4)	118.3(5)	117.81	118.32	117.87

Table 2 (*continued*)

Parameters	X-ray	B3LYP/6-311++G(d,p)		B3LYP-D3/6-311++G(d,p)
	1	**2** (vacuum)	**3** (DMSO)	**4** (vacuum)
C(14)—N(2)—O(5)	118.0(5)	117.80	118.20	117.98
O(4)—N(2)—O(5)	123.7(5)	124.39	123.42	124.14
C(21)—C(22)—C(23)	121.6(4)	122.08	122.42	122.45
C(21)—C(26)—C(25)	122.2(4)	122.18	120.08	122.22
C(22)—C(21)—C(26)	117.2(4)	116.69	116.51	116.30
C(22)—C(23)—C(24)	118.0(4)	118.73	118.84	118.64
C(23)—C(24)—C(25)	122.9(4)	121.67	121.63	121.56
C(24)—C(25)—C(26)	118.0(4)	118.64	118.52	118.82
C(22)—C(21)—O(6)	118.2(4)	125.36	125.65	125.94
C(26)—C(21)—O(6)	124.7(4)	117.94	117.84	117.76
Cl(3)—C(22)—C(21)	119.8(3)	118.98	119.22	119.25
Cl(3)—C(22)—C(23)	118.6(3)	118.93	118.70	118.29
Cl(4)—C(26)—C(21)	118.0(3)	118.53	118.43	118.71
Cl(4)—C(26)—C(25)	119.8(4)	119.29	119.15	119.06
N(3)—C(24)—C(23)	117.8(4)	119.15	119.17	119.17
N(3)—C(24)—C(25)	119.1(4)	119.17	119.20	118.27
C(24)—N(3)—O(8)	119.1(5)	117.78	118.30	117.67
C(24)—N(3)—O(7)	117.8(5)	117.73	118.24	117.68
O(7)—N(3)—O(8)	123.1(4)	124.49	123.46	123.65
Av. dif.[a]		−0.065	−0.020	0.055
R.m.s.[b]		−2.25	2.223	2.246
Selected torsion angles				
C(7)—N(1)—C(1)—C(2)	−118.3(4)	−115.08	−110.28	−115.60
C(7)—N(1)—C(1)—C(6)	62.0(4)	63.67	66.94	64.37
C(8)—N(1)—C(1)—C(2)	1.6(5)	3.65	8.15	3.49
C(8)—N(1)—C(1)—C(6)	−178.1(4)	−177.61	−174.63	−176.54
C(9)—N(1)—C(1)—C(2)	125.0(4)	125.96	131.37	126.04
C(9)—N(1)—C(1)—C(6)	−54.7(4)	−55.30	−51.41	−53.99
N(1)—C(1)—C(2)—C(3)	−177.7(4)	178.61	177.57	179.59
C(1)—C(2)—C(3)—C(4)	0.2(7)	0.12	−0.03	0.25
C(2)—C(3)—C(4)—C(5)	−1.8(7)	0.05	0.16	−0.01
C(3)—C(4)—C(5)—C(6)	1.3(7)	−0.22	−0.04	−0.12
C(4)—C(5)—C(6)—C(1)	0.8(7)	0.23	0.41	−0.00
C(6)—C(1)—C(2)—C(3)	2.0(6)	−0.10	0.41	−0.38
C(2)—C(1)—C(6)—C(5)	−2.5(6)	−0.07	−0.61	0.62
N(1)—C(1)—C(6)—C(5)	177.2(4)	−178.22	−177.84	−179.71
C(1)—N(1)—C(9)—C(10)	−50.9(4)	−53.49	−59.20	−51.80
C(7)—N(1)—C(9)—C(10)	−170.3(3)	−178.57	−177.82	−170.47
C(8)—N(1)—C(9)—C(10)	74.0(4)	65.41	66.43	73.04
N(1)—C(9)—C(10)—O(1)	141.7(4)	174.99	176.11	151.91
N(1)—C(9)—C(10)—O(2)	−40.7(5)	−5.66	−4.54	−28.85
C(9)—C(10)—O(1)—O(3)	177.8(2)	179.24	167.81	−172.50
C(9)—C(10)—O(2)—O(6)	−163.0(3)	−137.70	−156.47	−159.49
C(10)—O(1)—O(3)—C(11)	43.3(5)	119.58	97.85	26.39
C(10)—O(2)—O(6)—C(22)	−111.7(7)	−100.73	−102.34	−138.96
C(13)—C(12)—C(11)—O(3)	−179.2(4)	179.66	179.88	−178.30
Cl(1)—C(12)—C(11)—O(3)	1.5(5)	0.16	1.13	3.14
C(15)—C(16)—C(11)—O(3)	179.5(4)	−179.62	−179.91	177.82
Cl(2)—C(16)—C(11)—O(3)	−0.5(6)	83.42	0.24	−1.48
C(13)—C(14)—N(2)—O(4)	−6.3(7)	−0.52	−0.36	1.65
C(13)—C(14)—N(2)—O(5)	174.5(4)	179.45	179.68	−177.18
C(15)—C(14)—N(2)—O(4)	175.0(5)	179.64	179.95	−179.80
C(15)—C(14)—N(2)—O(5)	−4.2(6)	−0.39	−0.01	1.39
C(23)—C(22)—C(21)—O(6)	−177.5(4)	−179.35	179.84	178.92
Cl(3)—C(22)—C(21)—O(6)	0.6(5)	0.24	−0.30	−0.03
C(25)—C(26)—C(21)—O(6)	177.2(4)	179.30	−179.85	−178.91
Cl(4)—C(26)—C(21)—O(6)	−2.1(6)	−0.61	−179.85	0.56
C(23)—C(24)—N(3)—O(7)	1.8(7)	−0.05	0.03	−0.84
C(23)—C(24)—N(3)—O(8)	−179.7(4)	−179.90	−179.98	180.00
C(25)—C(24)—N(3)—O(7)	−179.4(5)	179.51	179.96	176.49
C(25)—C(24)—N(3)—O(8)	−0.9(7)	−0.34	−0.06	−0.67
Av. dif.[a]		−11.94	0.25	8.60
R.m.s.[b]		129.12	146.88	172.99

[a] Av. dif., average (signed) differences between experimental and scaling computed bond lengths and angels.
[b] Root-mean-square error.

2.452(4) and 2.623(4) Å. In the investigated complex **1** the C(10)—O(1) and C(10)—O(2) bond lengths of 1.257(5) and 1.230(5) Å, respectively, confirm the zwitterionic character of DMPB. The fact that the bond C(10)—O(1) is significantly longer than C(10)—O(2) is consistent with different interactions of the oxygen atoms, as explained below. The oxygen and chlorine atoms are get involved with the ring protons in short contacts, which have a character of weak H-bonds CH···O and CH···Cl (Table 3).

In the crystal, the carboxylate group acts as a double H-acceptor into two independent H-bonds. In this way three neutral molecules

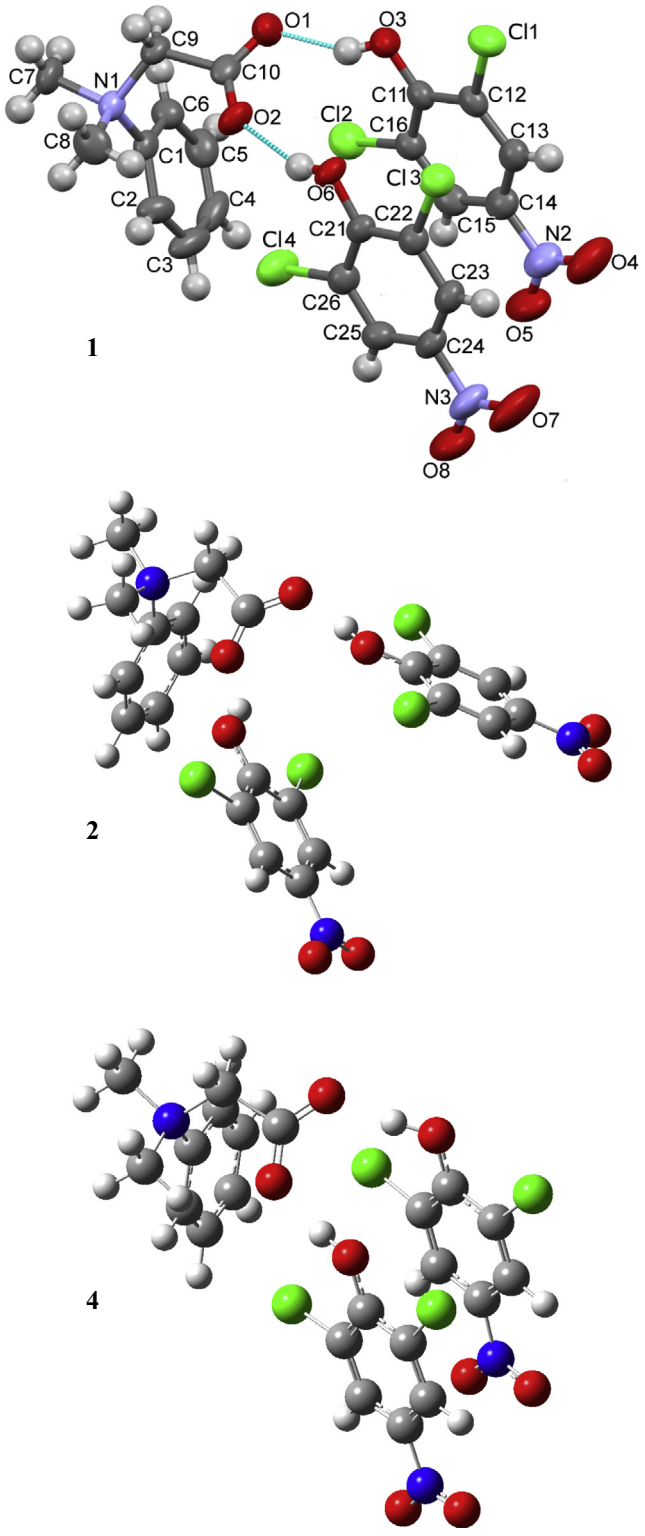

Fig. 1. The Hydrogen-bonding scheme and atom labeling in the crystal of the 1:2 complex of dimethylphenyl betaine with 2,6-dichloro-4-nitro-phenol (**1**), DMPB·$(DCNP)_2$; the optimized structure of **2** in vacuum and dispersion-correlated functional (D3) **4** by the B3LYP/6-311++G(d,p) approach.

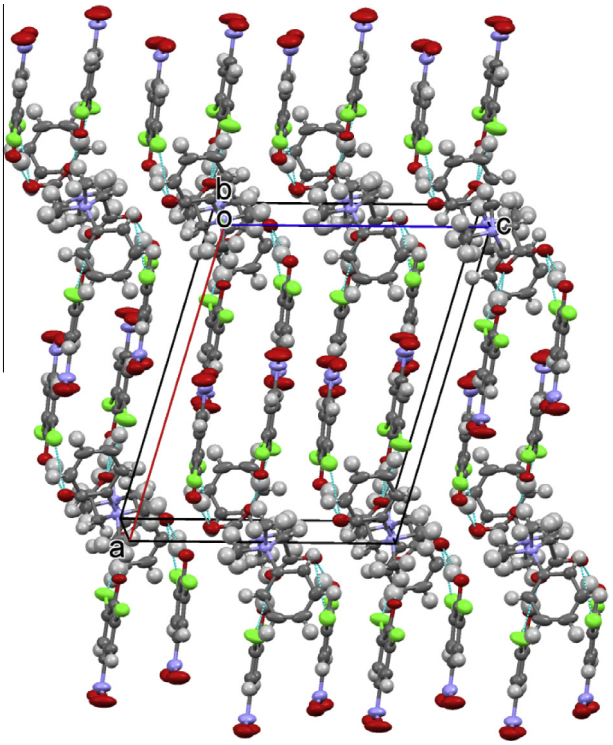

Fig. 2. Autostereogram [60] of molecules in the crystal structure of 1:2 complex of DMPB·$(DCNP)_2$.

aggregate to form the DMPB·$(DCNP)_2$ complex. The protons at the hydroxyl group of the phenols are H-bonded to both oxygen atoms of the carboxylate group of the DMPB. The dimensions of these OH···O bonds, listed in Table 3, show that the bond O(3)H···O(1) is significantly shorter, by 0.215(6) Å, than the bond O(6)H···O(2). In both these H-bonds the hydrogen atoms are located at similar distances, of about 0.85 Å (uncorrected), to the phenol oxygens. This strongly suggests that the difference in the O···O distances can result from the crystal environment inducing strains in the H-bridges. the is not confirmed by O—H···O angles, which are about 152°. However, the Donohue angles [33–35] clearly indicate that the O(3)H···O(1) bond is more relaxed: the C(11)—O(3)···O(1) angle is 128.4(3)° and C(10)—O(1)···O(3) 121.7(3)°, i.e. close to the optimal opening of about 120°, consistently with the oxygen atoms hybridization [36,37]. In the other hand, H-bond Donohue angles C(21)—O(6)···O(2) of 132.8(3)° and C(10)—O(2)···O(6) of 139.2(3)° considerably divert from the C—O···O angle opening favoured by the oxygens hybridization. Moreover, the torsion angle C(11)—O(3)···O(1)—C(10) across the H-bond is of 43.3(5)° and much closer to the planar arrangement than the C(21)—O(6)···O(2)—C(10) torsion angle, of −123.6(5)°, closer to the perpendicular arrangement of H-bonded groups. Moreover, there is also a significant difference in the torsion angles of the nitro groups with respect to the phenol ring: the N(2)O_2 group is inclined by 1.3° compared to the group N(3)O_2, inclined by 5.3°. This difference is significant for the charge distribution in the phenol molecule, because the highly electronegative NO_2 group closer to the phenyl ring is stronger conjugated with the aromatic ring and contribute more electrons to the molecule. This would be consistent with somewhat longer N(2)—O bonds and shorter bond C—N(2) than the corresponding bonds in the N(3)O_2 group.

Conformation of the investigated complex can be described by four planes A–D, fitted to the phenyl ring in DMPB (plane A: C(1)—C(2)—C(3)—C(4)—C(5)—C(6)), carboxyl group of DMPB (plane B: C(9)—C(10)—O(1)—O(2)) and two phenyl rings of DCNP (plane C: C(11)—C(12)—C(13)—C(14)—C(15)—C(16)) and (plane D: C(21)—C(22)—C(23)—C(24)—C(25)—C(26)). The dihedral angle

Table 3
OH···O hydrogen bond distances (Å), angels (°), energies (Hartree, a.u.) and dipole moments (μ, Debye) in the crystal (**1**), in vacuum (**2**), (**4**) and solvated by DMSO (**3**) for the 1:2 complex of dimethylphenyl betaine with 2,6-dichloro-4-nitro-phenol.

Compounds	D—H···A	d(D—H)	d(H···A)	d(D···A)	<(DHA)
1 – X-ray (Fig. 1)	O(3)—H(O3)···O(1)	0.83(6)	1.72(6)	2.473(5)	151(6)
	O(6)—H(O6)···O(2)	0.88(6)	1.88(6)	2.688(4)	153(5)
	C(4)—H···O(8)[d]	0.93	2.635	3.525(6)	160.37
	C(9)—H···O(2)[e]	0.97	2.500	3.337(5)	144.41
	C(9)—H···O(6)[e]	0.97	2.531	3.410(5)	150.58
	C(25)—H···O(4)[d]	0.93	2.678	3.562(7)	159.00
	C(7)—H···O(3)[f]	0.96	2.530	3.480(6)	170.49
	C(13)—H···O(8)[g]	0.93	2.706	3.578(7)	156.51
	C(9)—H···Cl(1)[g]	0.97	2.876	3.651(4)	137.59
	C(2)—H···Cl(2)[h]	0.93	2.807	3.633(5)	148.56
B3LYP/6-311++G(d,p)					
2 Vacuum[a]	O(3)—H(O3)···O(1)	0.999	1.667	2.629	159.90
	O(6)—H(O6)···O(2)	0.993	1.706	2.611	149.42
3 DMSO[b]	O(3)—H(O3)···O(1)	1.017	1.572	2.555	160.92
	O(6)—H(O6)···O(2)	1.007	1.625	2.576	155.52
B3LYP-D3/6-311++G(d,p)					
4 Vacuum[c]	O(3)—H(O3)···O(1)	1.003	1.623	2.611	167.80
	O(6)—H(O6)···O(2)	0.997	1.658	2.617	160.11

[a] Energy −3456.9741656 (Hartree, a.u.), dipole moment 24.6114 (μ, Debye).
[b] Energy −3457.0207845 (Hartree, a.u.), dipole moment 30.5884 (μ, Debye).
[c] Energy −3456.9612715 (Hartree, a.u.), dipole moment 22.3056 (μ, Debye).
Symmetry codes:
[d] 1 − *x*, −0.5 + *y*, 0.5 − *z*.
[e] −*x*, 1 − *y*, −*z*.
[f] −*x*, −0.5 + *y*, 0.5 − *z*.
[g] 1 − *x*, 0.5 + *y*, 0.5 − *z*.
[h] *x*, 1.5 − *y*, 0.5 + *z*.

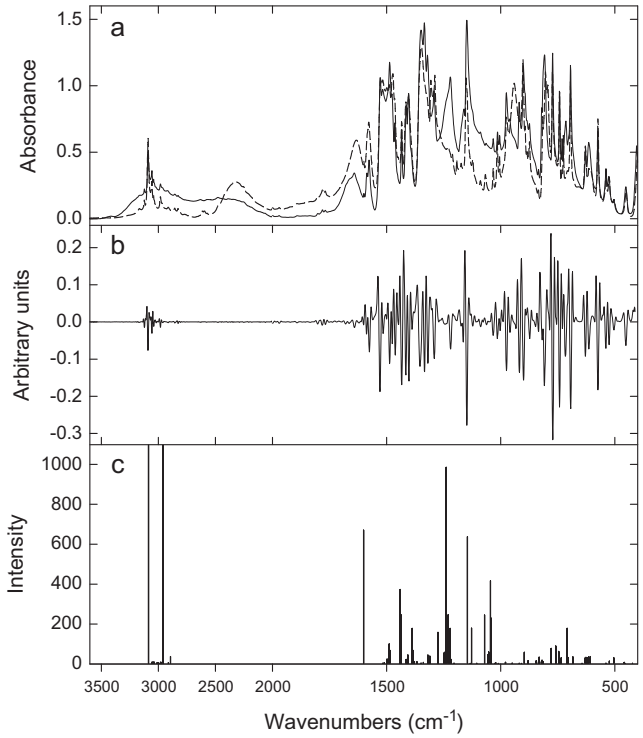

Fig. 3. Spectra of DMPB·(DCNP)$_2$: (a) solid line denotes FTIR (suspension in Nujol and Fluorolube) spectrum of **1** and the dashed line deuterated sample, (b) its second derivative (d^2) spectrum of **1**, (c) calculated and scaled spectrum of (**2**).

between the CH_2COO and phenyl ring in DMPB is 64.70°. The dihedral angles between planes are: AC (72.83°), AD (73.85°), BC (67.79°) and BD (64.45°). The two DCNP residues in the complex are nearly parallel; the dihedral angle is 3.59°.

Optimized structures

The structure of the 1:2 complex of DMPB·(DCNP)$_2$ in vacuum (**2**), in DMSO solution (**3**) were optimized by the B3LYP/6-311++G(d,p) approach (Table 2). Because in the structure **2** the two DCNP rings diverged strongly from the parallel arrangement observed in the crystal **1,** additional optimization with dispersion-corrected functional (B3LYP-D3) have been performed yielding structure **4.** The crystal structure **1** and the optimized structures **2** and **4** are compared in Fig. 1. The X-ray geometry was used as a starting point for these calculations. The calculated bond lengths and angles, except H-bonds, are in a good agreement with the X-ray data (Table 2). In the complexes **2**, **3** and **4** similarly as in **1**, the proton from DCNP is not transferred to DMPB, however the O—H···O distances of 2.629 and 2.611 Å in **2**, 2.555 and 2.576 Å in **3** and 2.611 and 2.617 in **4** suggest that the arrangement of the molecules in the optimized structures are more symmetric than in the crystal. Both H-bonds in the theoretically predicted structures **2** (in vacuum), **3** (in DMSO solution) and **4** (dispersion-corrected functional (D3)) are comparable but slightly shorter than O(6)—H(O6)···O(2) and much longer than O(3)—H(O3)···O(1) in the crystal **1** (Table 3). The angles between phenol rings are 29°, 22° and 7.5° respectively in **2**, **3** and **4**. It is worth noting that B3LYP-D3 method leads to a good agreement with the 3.59° observed in the crystal structure **1**.

The experimental and computed IR spectra

The experimental FTIR spectra of the complex of DMPB with two molecules of DCNP (**1**) and its deuterated derivative (**1a**) are shown in Fig. 3 and their frequencies are listed in Table 4. The broad absorption in the range 3400–2000 cm^{-1} (center of gravity at 2766 cm^{-1}) corresponds to the νOH vibrations in the longer H-bond. On deuteration it shifts to 2316 cm^{-1}. The broad absorption in the 1800–500 cm^{-1} region (center of gravity at

Table 4
Observed (FTIR and Raman) and calculated (B3LYP/6-311++G(d,p) (**2**) frequencies (cm^{-1}), infrared intensities (A_{cal}) and tentative assignments of bands in the 1:2 complex of dimethylphenyl-betaine with 2,6-dichloro-4-nitro-phenol (**1** and **2**) and their deuterated analogues (**1a** and **2a**).

1			**2**					**1a**		**2a**				
Raman	FT-IR	d^2	ν_{cal}	A_{cal}	ν_{scaleq}[a]	ν_{scalf}[b]	Assignment[c]	FT-IR	d^2	ν_{cal}	A_{cal}	ν_{scaleq}[d]	ν_{scalf}[b]	Assignment[c]
	3400–2000						νOH	2500–2000						νOD
3123	3122	3123	3276	2244.96	3084	3210	νOH	3124	3123	3239	0.16	3058	3174	νCH
			3239	0.23	3049	3174	νCH			3230	9.15	3049	3165	νCH
3093	3091	3091	3233	9.38	3043	3168	νCH	3091	3091	3233	9.17	3052	3168	νCH
3072	3057	3057	3232	9.81	3042	3167	νCH	3058	3057	3232	10.10	3051	3167	νCH
			3232	7.80	3042	3167	νCH	3044	3042	3231	8.79	3050	3166	νCH
3037	3042	3040	3231	7.96	3041	3166	νCH	3024	3022	3205	1.52	3025	3141	νCH
3020	3023	3019	3205	1.60	3016	3141	νCH	3006		3198	7.43	3018	3134	νCH
			3198	6.20	3010	3134	νCH	2983	2983	3190	11.01	3011	3126	νCH + $\nu_{as}CH_3$
2984	2982	2982	3190	9.84	3002	3126	νCH + $\nu_{as}CH_3$	2971	2966	3189	6.87	3010	3125	νCH + $\nu_{as}CH_3$
2963	2970	2966	3189	7.05	3001	3125	νCH + $\nu_{as}CH_3$			3180	0.06	3001	3116	νCH
			3181	0.04	2993	3117	νCH			3176	3.74	2997	3112	$\nu_{as}CH_3$
2921			3176	3.34	2988	3112	$\nu_{as}CH_3$	2856	2856	3163	12.36	2985	3100	$\nu_{as}CH + \nu_{as}CH_2$
2860	2856	2861	3163	9.72	2976	3100	$\nu_{as}CH_3$			3159	3.59	2981	3096	$\nu_{as}CH + \nu_{as}CH_2$
			3159	2.13	2972	3096	$\nu_{as}CH_3$			3155	0.55	2977	3092	$\nu_{as}CH_3$
			3155	0.19	2968	3092	$\nu_{as}CH_3$	2829	2828	3094	5.49	2918	3032	ν_sCH_2
2809	2828	2828	3142	2307.33	2956	3079	νOH			3075	25.66	2900	3014	ν_sCH_3
			3094	6.25	2910	3032	ν_sCH_2			3069	1.51	2894	3008	ν_sCH_3
			3075	37.65	2892	3014	ν_sCH_3			2396	1133.27	2248	2348	νOD
			3069	1.51	2886	3008	ν_sCH_3			2304	1147.27	2160	2258	νOD
1690	1642	1641	1729	670.94	1603	1694	ν_sCOO	1633	1632	1720	777.03	1600	1686	$\nu_{as}COO$
	1599	1601	1642	4.15	1519	1609	νCC	1600	1600	1641	4.08	1524	1608	νCC
	1586	1588	1635	6.10	1513	1602	νCC		1584	1635	5.92	1518	1602	νCC
1579	1577	1576	1622	25.39	1500	1590	νCC + $\nu_{as}NO_2$	1578	1577	1620	35.45	1504	1588	νCC + $\nu_{as}NO_2$
	1528	1529	1620	21.73	1498	1588	νCC + $\nu_{as}NO_2$	1527	1528	1618	39.90	1502	1586	νCC + $\nu_{as}NO_2$
	1517	1515	1612	100.79	1491	1580	νCC + $\nu_{as}NO_2$	1517	1515	1612	107.79	1496	1580	νCC + $\nu_{as}NO_2$
			1609	68.93	1488	1577	νCC + $\nu_{as}NO_2$	1500		1608	91.33	1492	1576	νCC + $\nu_{as}NO_2$
	1500–500						ν_{as}(OHO) + γOH	1500–500						ν_{as}(ODO) + γOD
1488	1487	1487	1562	373.46	1443	1531	νCC + $\nu_{as}NO_2$	1488	1488	1560	322.08	1446	1529	νCC + $\nu_{as}NO_2$
	1476	1475	1558	246.98	1439	1527	νCC + $\nu_{as}NO_2$	1473	1473	1557	259.28	1443	1526	νCC + $\nu_{as}NO_2$
			1534	22.96	1416	1503	δCH_3			1534	23.54	1421	1503	δCH_3
1465	1464	1462	1527	46.03	1409	1496	δCH + δCH_3	1465	1464	1527	45.63	1414	1496	δCH + δCH_3
1453	1434	1434	1507	178.41	1390	1477	νCO + νCC	1435	1434	1506	15.54	1394	1476	$\delta CH_3 + \delta CH_2$
1414	1413	1415	1506	35.46	1389	1476	δCH_3	1418	1416	1501	279.12	1389	1471	νCO + δCH
	1403	1402	1502	67.65	1385	1472	νCO + δCH	1404	1402	1497	18.19	1386	1467	δCH_3
			1497	12.23	1380	1467	δCH_3			1496	101.09	1385	1466	νCO + δCH
		1388	1494	1.21	1378	1464	δCH + δCH_3			1494	1.63	1383	1464	δCH + δCH_3
			1486	11.27	1370	1456	δCH + δCH_3			1486	11.41	1375	1456	δCH + δCH_3
			1467	4.92	1352	1438	δCH_3			1467	7.91	1357	1438	δCH_3
			1456	8.10	1341	1427	$\delta CH_3 + \delta CH_2$			1456	10.34	1346	1427	$\delta CH_3 + \delta CH_2$
	1349	1354	1436	45.44	1322	1407	δCH + δOH + δCH_2	1348	1356	1432	29.87	1323	1403	δCH + δCH_3
1337	1334	1334	1434	19.14	1320	1405	δCH + δOH + δCH_2 + δCC		1346	1431	6.30	1322	1402	δCH + δCH_3 + δCC
	1320	1319	1427	39.78	1313	1398	δCH_3		1320	1427	44.43	1318	1398	δCH_3
1291	1293	1291	1390	158.52	1278	1362	$\nu_sCC + \delta CH_2 + \delta CH_3$	1288	1288	1388	236.44	1281	1360	νCO + δCH_2 + δCH_3
			1364	26.60	1253	1337	δCH			1363	0.91	1257	1336	δCH
			1362	56.38	1251	1335	δCH		1270	1356	969.69	1250	1329	ν_sNO_2
			1359	58.66	1248	1332	δOH + ν_sNO_2	1231	1229	1353	253.71	1247	1326	ν_sNO_2
1195	1221	1220	1352	985.69	1242	1325	$\delta CH_2 + \nu_sNO_2$	1192	1191	1345	0.86	1240	1318	δCH_2
1174	1161	1164	1345	247.63	1235	1318	δOH + δCH_2			1342	190.17	1237	1315	δCH + νCC
			1343	232.24	1233	1316	δOH + δCH_2			1339	108.15	1234	1312	δCH + νCC
			1335	178.48	1225	1308	γCH_2			1334	183.75	1229	1307	γCH_2
			1334	0.95	1224	1307	νCO + δCH			1320	40.34	1216	1294	δCH + νCC
			1330	23.13	1221	1303	νCC			1319	30.43	1215	1293	δCH + νCC
			1317	4.51	1208	1291	δCH_2			1317	6.09	1213	1291	δCH_2
			1255	637.64	1149	1230	δOH + δCH	1151	1150	1243	0.23	1142	1218	δCH_3
1152	1148	1148	1243	3.24	1137	1218	δCH_3			1220	1.4	1120	1196	δCH
1125		1122	1237	179.75	1131	1212	δOH + δCH	1122		1213	4.18	1113	1189	$\delta CH_3 + \delta CH_2$
		1088	1220	2.33	1115	1196	δCH			1211	17.38	1111	1187	δCH
1063			1213	3.86	1108	1189	$\delta CH_3 + \delta CH_2$			1209	6.78	1109	1185	δCH
			1192	0.06	1088	1168	δCH			1192	0.09	1093	1168	δCH
1033	1033	1033	1177	245.28	1074	1153	δOH + δCH	1032	1033	1161	9.50	1063	1138	δCH + δCH_3 + δCH_2
			1163	47.06	1061	1140	δOH			1152	195.83	1055	1129	δCC + νCCl
			1159	60.57	1057	1136	δOH + δCH_3 + δCH_2	1015	1015	1151	102.09	1054	1128	δCC + νCCl
	1014	1015	1150	416.85	1048	1127	δCH	1005		1132	0.47	1035	1109	δCH_3
	1005	1003	1147	230.23	1045	1124	δOH + δCH			1127	5.75	1031	1104	δCH + δCH_3
			1132	2.83	1031	1109	δCH_3			1115	3.16	1019	1093	δCH + δCH_3
			1126	6.60	1025	1103	δCH_3 + δCH			1083	15.29	988	1061	δCH
			1115	2.81	1015	1093	δCH_3 + δCH			1082	18.32	987	1060	δCH
			1083	6.70	984	1061	δCH	975	974	1052	5.60	959	1031	δCH
			1082	9.20	983	1060	δCH			1019	4.20	927	999	δCC

Table 4 (*continued*)

1			2					1a		2a				
Raman	FT-IR	d^2	ν_{cal}	A_{cal}	ν_{scaleq}[a]	ν_{scalf}[b]	Assignment[c]	FT-IR	d^2	ν_{cal}	A_{cal}	ν_{scaleq}[d]	ν_{scalf}[b]	Assignment[c]
977	975	975	1052	4.88	954	1031	δCH			1013	1.21	921	993	δCH
			1019	3.93	923	999	νCC			1010	1.69	918	990	$\delta CH_3 + \delta CH_2$
			1013	1.40	917	993	δCH			983	0.83	892	963	γCH
960	961	959	1010	2.94	914	990	$\delta CH_3 + \delta CH_2$			979	13.46	888	959	$\delta CH_3 + \delta CH_2$
		933	983	0.87	888	963	γCH	920		950	406.24	861	931	δOD
	919	918	979	16.76	884	959	γCH	902	902	939	95.15	850	920	δOD + skeletal
	901	901	942	16.32	849	923	γCH	874	873	934	18.56	845	915	Skeletal
888		873	932	3.22	839	913	νCN		834	928	7.59	840	909	δOD + $\nu CN(NO_2)$
874	835	834	931	10.62	838	912	νCN	816	817	924	49.48	836	906	δOD + δCH
821	820	819	929	33.97	836	910	γCH			918	58.19	830	900	δOD + δCH
			918	11.25	826	900	γCH			917	4.84	829	899	δOD + δCH
			915	19.40	823	897	γCH			914	32.55	826	896	γCH
			911	12.93	819	893	γCH			911	4.87	823	893	γCH
			910	6.24	818	892	γCH			910	2.86	822	892	γCH
			903	58.68	812	885	γCH	803	804	891	114.90	804	873	νCN (amine)
	808	809	874	78.27	784	857	γOH	793	792	853	54.20	768	836	νCN (amine)
		786	853	90.50	764	836	νCN amine	773	772	832	0.79	747	815	γCH
	773	772	840	62.89	751	823	γOH	742	742	829	65.28	744	812	δCC
734	742	742	836	22.25	747	819	Skeletal	725	726	826	22.60	742	809	δCC
		730	833	5.18	745	816	γOH		712	792	217.17	709	776	νCCl + skeletal
713	715	716	828	31.30	740	811	γOH + γCH	694	694	787	59.33	704	771	νCCl + δOD + skeletal
	694	693	801	178.79	714	785	νCCl + skeletal	629	629	775	42.42	693	760	γCH
	629	631	798	32.83	711	782	νCCl + skeletal	613	612	735	4.95	654	720	γNO_2 + skeletal
614	615	614	775	36.22	689	760	γCH			734	6.25	653	719	γNO_2 + skeletal
			733	3.64	649	718	γNO_2			732	1.95	651	717	Skeletal
			732	0.40	648	717	γNO_2			723	14.09	643	709	γOD + skeletal
			731	0.36	647	716	Skeletal	574	574	718	19.15	638	704	γNO_2 + skeletal
573	574	574	719	31.44	635	705	δNO_2 + skeletal			714	17.68	634	700	Skeletal
			717	4.04	633	703	δNO_2 + skeletal			711	1.30	631	697	Skeletal
			715	33.86	632	701	Skeletal			709	9.82	629	695	Skeletal
			707	31.40	624	693	Skeletal	539	539	703	56.46	624	689	γCH
537	539	539	703	35.27	620	689	γCH	524	524	630	17.42	553	617	γOD + skeletal
	526	526	696	37.27	613	682	γOH + δCOO			629	33.82	553	616	γOD
			630	0.19	550	617	Skeletal			619	6.07	543	607	Skeletal
			627	1.84	547	614	Skeletal			612	6.57	536	600	Skeletal
			624	4.25	544	612	Skeletal			603	11.30	528	591	γOD + skeletal
			608	14.45	529	596	Skeletal	503	502	596	100.52	521	584	γOD + skeletal
503	504	504	588	32.16	510	576	γCH_2	450	450	578	6.44	504	566	γOD + skeletal
454	452	452	541	8.80	465	530	Skeletal			539	12.21	466	528	δCH_2 + skeletal
			539	3.76	463	528	Skeletal			536	0.51	463	525	Skeletal
405	404		538	4.37	462	527	δCH_2 + skeletal			535	7.09	462	524	Skeletal
			535	0.28	459	524	γCH			534	0.20	461	523	Skeletal
			533	0.61	457	522	γCH			533	0.63	460	522	Skeletal
			503	0.85	429	493	Skeletal			503	1.43	432	493	Skeletal
385			503	3.89	429	493	Skeletal			502	3.87	431	492	Skeletal
			502	0.49	428	492	Skeletal			501	1.40	430	491	Skeletal
			435	2.72	363	426	Skeletal			434	2.48	365	425	Skeletal
			416	0.60	345	408	Skeletal			416	0.60	348	408	Skeletal
			390	34.40	320	382	Skeletal			388	38.72	321	380	Skeletal
Av.dif.[e]			-116		0.07	-86				-112		0	-72	
R.m.s.[f]			58		47	50				56		44	41	

[a] Scaling equation: $\nu_{scaleq} = -53.2103 + 0.9577\ \nu_{calc}$, $r = 0.9982$.
[b] Scaling factor: 0.98.
[c] as – asymmetric, s – symmetric, ν – stretching, δ – deformation in-plane, γ – deformation out-of-plane.
[d] Scaling equation: $\nu_{scaleq} = -51.1870 + 0.9598\ \nu_{calc}$, $r = 0.9986$.
[e] Average (signed) differences between experimental and computed data;
[f] Root-mean-square errors.

1121 cm^{-1}) is attributed to the shorter H-bond. A similar broad absorption is observed in the IR spectra of 2:1 complexes of homarine [38], trigonelline [39], 1-methylisonicotinate inner salts [40] and Type A acid salts of carboxylic acids [41–43]. The broad absorption is typical of compounds with short H-bonds and is assigned to the ν_{as}(OHO) and γ(OH) vibrations of the short hydrogen bonds [42,43]. In the Raman spectrum the broad absorption is absent.

In the FTIR spectrum, the broad absorption overlaps with the narrow skeletal absorption, but the latter can be distinguished in the second-derivative, d^2 (Fig. 3b), or forth-derivative, d^4, spectra [44,45]. The minima in the d^2 spectrum have the same wavenumbers as the maxima in the absorbance spectrum. Since the relative intensities in the d^2 spectrum vary inversely to the square of the half-width ratio of the absorbance bands in the FTIR spectrum, the broad bands assigned to the O···H···O modes are not observed in the d^2 spectrum. The scaled frequencies of **2**, calculated by the B3LYP/6-311++G(d,p) approach, is shown in Fig. 3c as the vertical lines. The most intense lines at 3084 and 2956 cn^{-1} are assigned to the νOH vibration. In the calculated spectrum of the deuterated sample these bands appear at 2248 and 2160 cm^{-1} (Table 4). The isotope ratio of ν_H/ν_D of 1.37 confirms the O···O distances of ca. 2.6 Å. As Figs. 3b and 3c show that the calculated frequencies agree well with the negative d^2 bands. From this similarity we conclude

that the calculated data describe only the narrow skeletal frequencies without the broad absorption.

The overestimation of the computed wavenumbers is quite systematic and can be corrected by applying appropriate scaling factors or scaling equation [46–53]. Linear relations between the experimental and calculated scaled frequencies for DMPB·(DCNP)$_2$ (Fig. 4a) and its deuterated analogue (Fig. 4b) are characterized by a good correlation coefficient. This scaling procedure, as recommended by Alcolea Palafox [48], was used for adjusting the predicted frequencies, listed in Table 4 as ν_{scaled}. Scaling of the harmonic vibration frequencies reproduced the experimental solid FTIR frequencies with the r.m.s. error of 47 cm^{-1} in **2** and 44 cm^{-1} in **2a**. After scaling of the harmonic vibrational frequencies by a factor 0.98 (ν_{scalf}) [46] the r.m.s. error is 50 cm^{-1} for **2** and 41 cm^{-1} for **2a** (Table 4). The vibrational band assignments of **2** and **2a** was made using Gauss-View molecular visualization program [54]. There are no simple relations between the measured and calculated intensities of bands [55].

^{1}H and ^{13}C NMR spectra

The NMR spectra the complex of DMPB with two molecules of DCNP (**1**) in DMSO-d$_6$ solution are shown in Fig. 5. The assignments of carbon-13 and proton chemical shifts listed in Table 5, were based on two dimensional ^{1}H—^{1}H and ^{1}H—^{13}C experiments [56]. The relations between the experimental ^{13}C and ^{1}H chemical shifts (δ_{exp}) and the GIAO (Gauge-Independent Atomic Orbitals) magnetic isotropic shielding constants (σ_{calc}), which are widely used in an efficient implementation [57,58], are usually linear and described by the following equation: $\delta_{exp} = a + b\ \sigma_{calc}$. The slope and intercept of the least-squares correlation line is used to scale the GIAO magnetic isotropic shielding constants, σ_{calc},

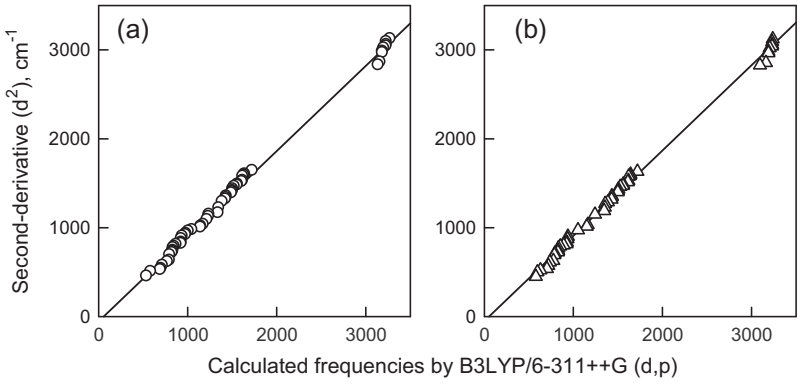

Fig. 4. Correlation between the experimental and calculated B3LYP/6-311++G(d,p) frequencies for DMPB·(DCNP)$_2$ (a) and deuterated sample (b).

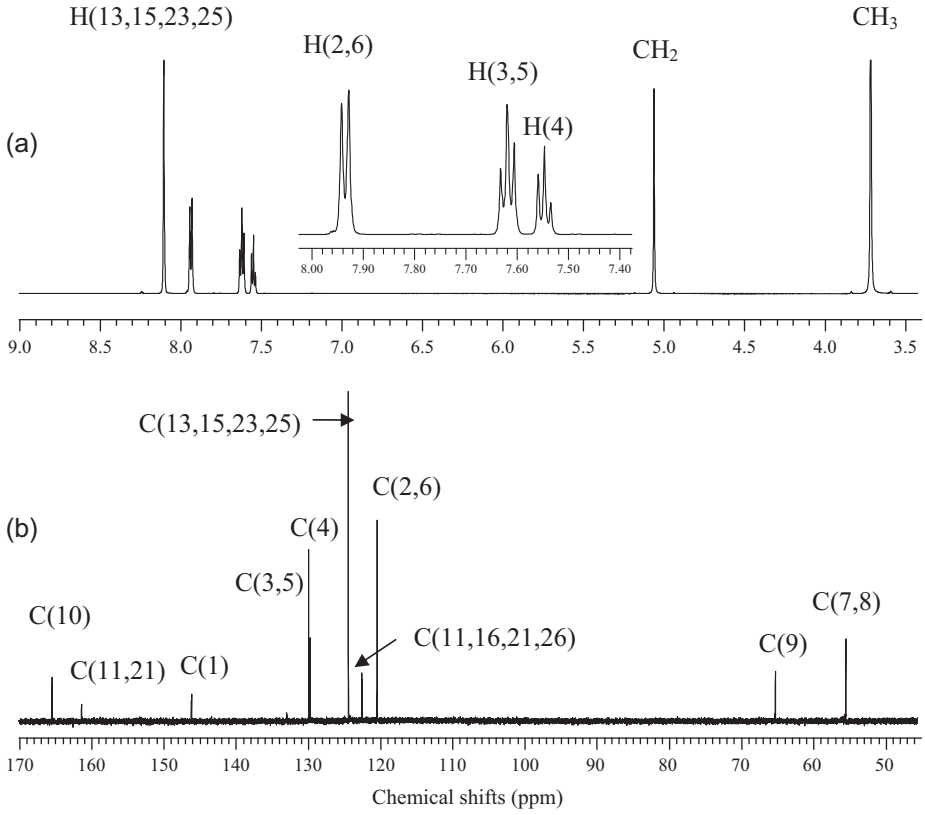

Fig. 5. NMR spectra of DMPB·(DCNP)$_2$ in DMSO-d$_6$ solution: (a) ^{1}H and (b) ^{13}C.

Table 5
Experimental and predicted ($\delta_{pred} = a + b\ \sigma_{calc}$) carbon-13 and proton chemical shifts (ppm) and calculated GIAO/B3LYP/6-311++G(d,p) isotropic magnetic shielding constants (σ_{calc}) for 1:2 complex of dimethylphenyl betaine with 2,6-dichloro-4-nitro-phenol in DMSO.

Atom	δ_{exp} **1**	δ_{pred} **3**	σ_{calc} **3**
Carbon-13			
C(1)	146.12	145.83	29.0088
C(2)	120.48	119.97	56.2981
C(3)	129.98	128.99	46.7757
C(4)	129.76	128.88	46.8997
C(5)	129.98	129.20	46.5542
C(6)	120.48	119.08	57.2334
C(7)	55.54	58.58	121.0635
C(8)	55.54	48.85	131.3191
C(9)	65.20	67.38	111.7706
C(10)	165.55	163.29	10.5948
C(11), C(21)	161.53	156.29	17.9786
C(12), C(22)	122.56	126.47	49.4412
C(13), C(23)	124.48	124.71	51.2897
C(14), C(24)	132.79	136.61	38.7402
C(15), C(25)	124.56	124.20	51.8295
C(16), C(26)	122.56	128.80	46.9742
a[a]		173.3310	
b[b]		−0.9479	
r[c]		0.9949	
Av. dif.[d]		0.86	
R.m.s.[e]		2.61	
Proton			
H(2)	7.94	7.86	23.9780
H(6)	7.94	7.72	24.1312
H(3)	7.62	7.81	24.0244
H(5)	7.62	7.83	24.0025
H(4)	7.55	7.78	24.0614
H(71–73) av	3.70	4.16	28.6780
H(81–83) av	3.70	4.66	28.0580
H(91–92) av	5.06	7.90	27.4988
H(13), H(23)	8.10	8.00	23.9240
H(15), H(25)	8.10	7.86	23.8165
a[a]		29.6016	
b[b]		−0.9069	
r[c]		0.9897	
Av. dif.[d]		−0.43	
R.m.s.[e]		0.92	

[a] Intercept.
[b] Slope.
[c] Correlation coefficient.
[d] Average (signed) differences between experimental and predicted chemical shifts.
[e] Root-mean-square errors.

and to predict the chemical shifts, $\delta_{pred} = a + b\ \sigma_{calc}$, (Fig. 6). The parameters *a* and *b* are listed in Table 5. The r.m.s. error for carbon-13 is 2.61 ppm and for hydrogen is 0.92 ppm. The magnetic isotropic shielding constants confirm the correct assignments of the chemical shifts to the appropriate atoms. The chemical shifts listed in Table 5 agree well with those in dimethylphenyl betaine monohydrate [19] and dimethylphenyl betaine hydrochloride [59].

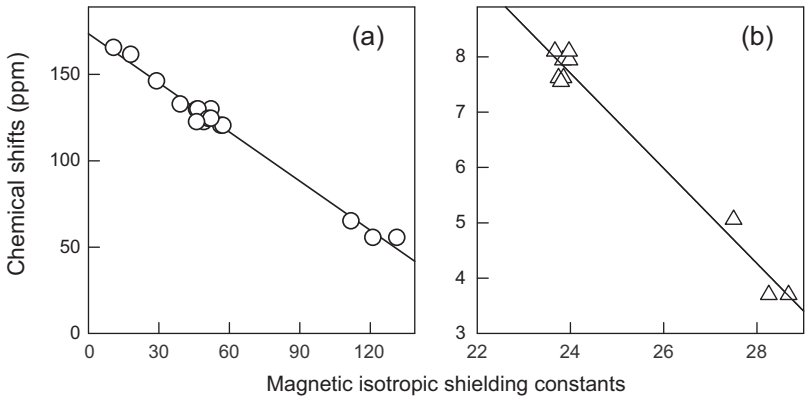

Fig. 6. Plot of the experimental ^{13}C (a) and ^{1}H (b) chemical shifts of **1** in DMSO-d_6 solutions versus the average magnetic isotropic shielding constants from GIAO/B3LYP/6-311++G(d,p) calculations for DMPB·$(DCNP)_2$ (**3**).

Conclusions

Dimethylphenyl betaine (DMPB) forms 1:2 complex with two molecules of 2,6-dichloro-4-nitro-phenol (DCNP). Phenols are bonded to each oxygen atom of DMPB carboxylate group by two nonequivalent H-bonds with the O—H···O distances of 2.473(5) and 2.688(4) Å without proton transfer. Both H-bond lengths in structures **2** (in vacuum), **3** (in DMSO solution) optimized by the B3LYP/6-311++G(d,p) approach and **4** (in vacuum) optimized by B3LYP-D3/6-311++G(d,p) approach are comparable but slightly shorter than O(6)—H(O6)···O(2) in the crystal. The FTIR spectrum of **1** shows a broad absorption in the 3400–2000 cm^{-1} region corresponding to the νOH vibration in the longer hydrogen bond and a broad absorption in 1800–500 cm^{-1} region attributed to the ν_{as} (OHO) and γ(OH) vibrations in the shorter H-bond. The relations between the experimental ^{13}C and ^{1}H chemical shifts (δ_{exp}) of the investigated compound **1** in DMSO-d_6 and GIAO/B3LYP/6-311++G(d,p) magnetic isotropic shielding constants (σ_{calc}) obtained by using the screening solvation model (COSMO) calculated for **3** are linear and described by the following equation: $\delta_{exp} = a + b\,\sigma_{calc}$ and confirm the correct assignments of the resonance signals. The angles between phenol rings are 3,59°, 37°, 15° and 7.5° respectively in **1**, **2**, **3** and **4**. The B3LYP-D3/6-311++G(d,p) approach better reproduces the crystal structure than the B3LYP/6-311++G(d,p) approach one.

Acknowledgements

The computations were performed in Poznań Supercomputing and Networking Centre and supported in part by PL-Grid Infrastructure.

Appendix A. Supplementary material

Supplementary data (Table S1) associated with this article can be found, in the online version, at http://dx.doi.org/10.1016/j.saa.2014.10.007.

References

[1] G.R. Desiraju, Angew. Chem. Int. Ed. 50 (2011) 52–59.
[2] S.J. Grabowski, Chem. Rev. 111 (2011) 2597–2625.
[3] B.G. de Oliveira, Phys. Chem. Chem. Phys. 15 (2013) 37–79.
[4] P. Goymer, Nat. Chem. 4 (2012) 863.
[5] G.A. Jeffrey, W.A. Saenger, Hydrogen Bonding in Biological Structure, Springer-Verlag, Berlin, 1991.
[6] G.R. Desiraju, T. Steiner, The Weak Hydrogen Bond in Structural Chemistry and Biology, University Press, Oxford, 2001.
[7] G. Gilli, P. Gilli, The Nature of the Hydrogen Bond, University Press, Oxford, 2009.
[8] H.D. Lutz, Struct. Bonding 69 (1988) 97–125.
[9] L. Sobczyk, S.J. Grabowski, T.M. Krygowski, Chem. Rev. 105 (2005) 3513–3660.
[10] X. Domingo, Betaines, in: E.G. Lomax (Ed.), Amphoteric Surfactants, Marcel Dekker, New York, 1996, pp. 76–190.
[11] A. Schmidt, Adv. Heterocycl. Chem. 85 (2003) 67–171.
[12] E. Alcalde, Adv. Heterocycl. Chem. 60 (1994) 197–259.
[13] S.A.S. Craig, Am. J. Clin. Nutr. 80 (2004) 539–549.
[14] M. Szafran, I. Kowalczyk, A. Katrusiak, Z. Dega-Szafran, J. Mol. Struct. 651–653 (2003) 621–634. and Ref. cited therein..
[15] D. Godzisz, M.M. Ilczyszyn, M. Ilczyszyn, J. Mol. Struct. 606 (2002) 123–137. and Ref. cited therein..
[16] Z. Dega-Szafran, E. Sokolowska, J. Mol. Struct. 565–566 (2001) 17–23. and Ref. cited therein.
[17] M. Szafran, Z. Dega-Szafran, G. Buczak, A. Katrusiak, M.J. Potrzebowski, A. Komasa, J. Mol. Struct. 416 (1997) 145–160.
[18] G. Buczak, Z. Dega-Szafran, A. Katrusiak, M. Szafran, J. Mol. Struct. 436–437 (1997) 143–151.
[19] M. Szafran, K. Ostrowska, A. Katrusiak, Z. Dega-Szafran, Spectrochim. Acta A 128 (2014) 844–851.
[20] G.S. Sheldrick, Acta Crystallogr. A64 (2008) 112–122.
[21] C.K. Johnson, ORTEPII, Report ORNL-5138, Oak Ridge National Laboratory, Tennessee, USA, 1975.
[22] Stereochemical Workstation Operation Manual, Release 3.4, Siemens Analytical X-ray Instruments Inc., Madison, 1989.
[23] M.J. Frisch, G.W. Trucks, H.B. Schlegel, G.E. Scuseria, M.A. Robb, J.R. Cheeseman, G. Scalmani, V. Barone, B. Mennucci, G.A. Petersson, H. Nakatsuji, M. Caricato, X. Li, H.P. Hratchian, A.F. Izmaylov, J. Bloino, G. Zheng, J.L. Sonnenberg, M. Hada, M. Ehara, K. Toyota, R. Fukuda, J. Hasegawa, M. Ishida, T. Nakajima, Y. Honda, O. Kitao, H. Nakai, T. Vreven, J.A. Montgomery Jr., J.E. Peralta, F. Ogliaro, M. Bearpark, J.J. Heyd, E. Brothers, K.N. Kudin, V.N. Staroverov, R. Kobayashi, J. Normand, K. Raghavachari, A. Rendell, J.C. Burant, S.S. Iyengar, J. Tomasi, M. Cossi, N. Rega, N.J. Millam, M. Klene, J.E. Knox, J.B. Cross, V. Bakken, C. Adamo, J. Jaramillo, R. Gomperts, R.E. Stratmann, O. Yazyev, A.J. Austin, R. Cammi, C. Pomelli, J.W. Ochterski, R.J. Martin, K. Morokuma, V.G. Zakrzewski, G.A. Voth, P. Salvador, J.J. Dannenberg, S. Dapprich, D.A. Daniels, O. Farkas, J.B. Foresman, J.V. Ortiz, J. Cioslowski, D.J. Fox, GAUSSIAN 09, Revision B.01 Gaussian Inc., Wallingford CT, 2009.
[24] A.D. Becke, Chem. Phys. 107 (1997) 8554–8580. and Ref. cited therein.
[25] P.J. Stephensen, F.J. Devlin, C.F. Chabalowski, M. Fisher, J. Phys. Chem. 98 (1994) 11623–11810.
[26] S. Grimme, J. Antony, S. Ehrlich, H. Krieg, J. Chem. Phys. 132 (2010) 154104.
[27] W.J. Hehre, L. Random, P.V.R. Schleyer, J.A. Pople, Ab Initio Molecular Orbital Theory, Wiley, New York, 1989.
[28] V. Barone, M. Cossi, J. Phys. Chem. A 102 (1998) 1995–2001.
[29] G. Brancato, N. Rega, V. Barone, J. Chem. Phys. 125 (2006) 16515–16525.
[30] K. Wolinski, J.F. Hilton, P. Pulay, J. Am. Chem. Soc. 112 (1990) 8251–8260.
[31] P. Pulay, X. Zhou, F. Fogarasi, in: R. Fausto (Ed.), Recent Experimental and Computational Advances in Molecular Spectroscopy, Kluver, Academic, Netherlands, 1993, pp. 88–111.
[32] A. Klam, COSMO-RS from Quantum Chemistry to Fluid Phase Thermodynamics and Drug Design, Elsevier, Amsterdam, 2005.
[33] A. Katrusiak, J. Mol. Struct. 374 (1996) 177–189.
[34] R. Gajda, A. Katrusiak, J. Crassous, Cryst. Eng. Comm. 11 (2009) 2668–2676.
[35] W. Cai, A. Katrusiak, Cryst. Eng. Comm. 14 (2012) 42420–44424.
[36] A. Katrusiak, Phys. Rev. B 48 (1993) 2992–3002.
[37] M. Ratajczak-Sitarz, A. Katrusiak, J. Mol. Struct. 995 (2011) 29–34.
[38] M. Szafran, A. Katrusiak, Z. Dega-Szafran, J. Mol. Struct. 839 (2007) 99–106.
[39] M. Szafran, A. Katrusiak, J. Koput, Z. Dega-Szafran, J. Mol. Struct. 784 (2006) 98–108.
[40] M. Szafran, A. Katrusiak, Z. Dega-Szafran, J. Mol. Struct. 880 (2008) 77–85.
[41] D. Hadži, S. Bratos, in: P. Schuster, G. Zundel, C. Sandorfy (Eds.), The Hydrogen Bond, Recent Development and Experiments, vol. 2, North-Holland, Amsterdam, 1976, pp. 565–611.
[42] A. Novak, Struct. Bond. 18 (1974) 177–215.
[43] J. Baran, M. Drozd, T. Głowiak, M. Śledź, H. Ratajczak, J. Mol. Struct. 372 (1995) 131–144.
[44] W.F. Maddams, M.J. Southon, Spectrochim. Acta A 38A (1982) 459–486.
[45] G. Talski, Derivative Spectrophotometry, Wiley-VCH, Weinheim, Germany, 1994.
[46] A.P. Scott, L. Radom, J. Phys. Chem. 100 (1996) 16502–16513.
[47] M. Alcolea Palafox, Int. J. Quant. Chem. 77 (2000) 661–684.
[48] M. Alcolea Palafox, V.K. Rastogi, Spectrochim. Acta A58 (2002) 411–440.
[49] K. Szczepaniak, M.M. Szcześniak, W.B. Person, J. Phys. Chem. A104 (2000) 3852–3863.
[50] K. Szczepaniak, W.B. Person, D. Hadži, J. Phys. Chem. A109 (2005) 6710–6724.
[51] M. Alcolea Palafox, M. Gill, N.J. Nunez, V.K. Rastogi, L. Mittal, R. Sharma, Int. J. Quant. Chem. 103 (2005) 394–421.
[52] Y.I. Binev, M.K. Georgieva, L.I. Daskalova, Spectrochim. Acta A60 (2004) 2601–2610.
[53] M. Szafran, E. Bartoszak-Adamska, J. Koput, Z. Dega-Szafran, J. Mol. Struct. 844–845 (2007) 140–156.
[54] R. Dennington II, T. Keith, J. Millam, Gauss View, Version 4.1.2, Semichem, Inc., Shawnee Mission, KS, 2007.
[55] M.T. Rosado, M.L.T.S. Duarte, R. Fausto, Vibr. Spectr. 16 (1998) 35–54.
[56] J.H. Simpson, Organic Structure Determination Using 2-D NMR Spectroscopy, Academic Press, Elsevier, Amsterdam, 2008.
[57] R. Dichfield, Mol. Phys. 27 (1974) 789–807.
[58] B. Ośmialowski, E. Kolehmainen, R. Gawinecki, Magn. Res. Chem. 39 (2001) 334–340.
[59] M. Szafran, A. Katrusiak, Z. Dega-Szafran, I. Kowalczyk, J. Mol. Struct. 1031 (2013) 49–55.
[60] A. Katrusiak, J. Mol. Graph. Model. 19 (2001) 363–367.